

Multi-replica biased sampling for photoswitchable π -conjugated polymers

Mariagrazia Fortino¹, Concetta Cozza¹, Massimiliano Bonomi^{2,*}, Adriana Pietropaolo^{3,*}

AFFILIATIONS

¹ Dipartimento di Scienze della Salute, Università di Catanzaro, Viale Europa, 88100 Catanzaro, Italy.

²Structural Bioinformatics Unit, Department of Structural Biology and Chemistry; CNRS UMR 3528; C3BI, CNRS USR 3756; Institut Pasteur, Paris, France. ORCID: 0000-0002-7321-0004.

³Dipartimento di Scienze della Salute, Università di Catanzaro, Viale Europa, 88100 Catanzaro, Italy. ORCID: 0000-0003-0955-2058

*** Authors to whom correspondence should be addressed:**

apietropaolo@unicz.it, mbonomi@pasteur.fr

ABSTRACT

In recent years, π -conjugated polymers are attracting considerable interest in view of their light-dependent torsional reorganization around the π -conjugated backbone, which determines peculiar light-emitting properties. Motivated by the interest in designing conjugated polymers with tunable photoswitchable pathways, we devised a computational framework to enhance the sampling of the torsional conformational space and at the same time estimate ground to excited-state free-energy differences. This scheme is based on a combination of Hamiltonian Replica Exchange (REM), Parallel Bias metadynamics, and free-energy perturbation theory. In our scheme, each REM replica samples an intermediate unphysical state between the ground and the first two excited states, which are characterized by TD-DFT simulations at the B3LYP/6-31G* level of theory. We applied the method to a 5-mer of 9,9-dioctylfluorene and found that upon irradiation this system can undergo a dihedral inversion from -155 to 155 degrees crossing a barrier that decreases from 0.1 eV in the ground state (S_0) to 0.05 eV and 0.04 eV in the first (S_1) and second (S_2) excited states. Furthermore, S_1 and even more S_2 were predicted to stabilize coplanar dihedrals, with a local free-energy minimum located at ± 44 degrees. The presence of a free-energy barrier of 0.08 eV for the S_1 and 0.12 eV for the S_2 state can trap this conformation in a basin far from the global free-energy minimum located at 155 degrees. The simulation results were compared with the experimental emission spectrum, showing a quantitative agreement with the predictions provided by our framework.

I. INTRODUCTION

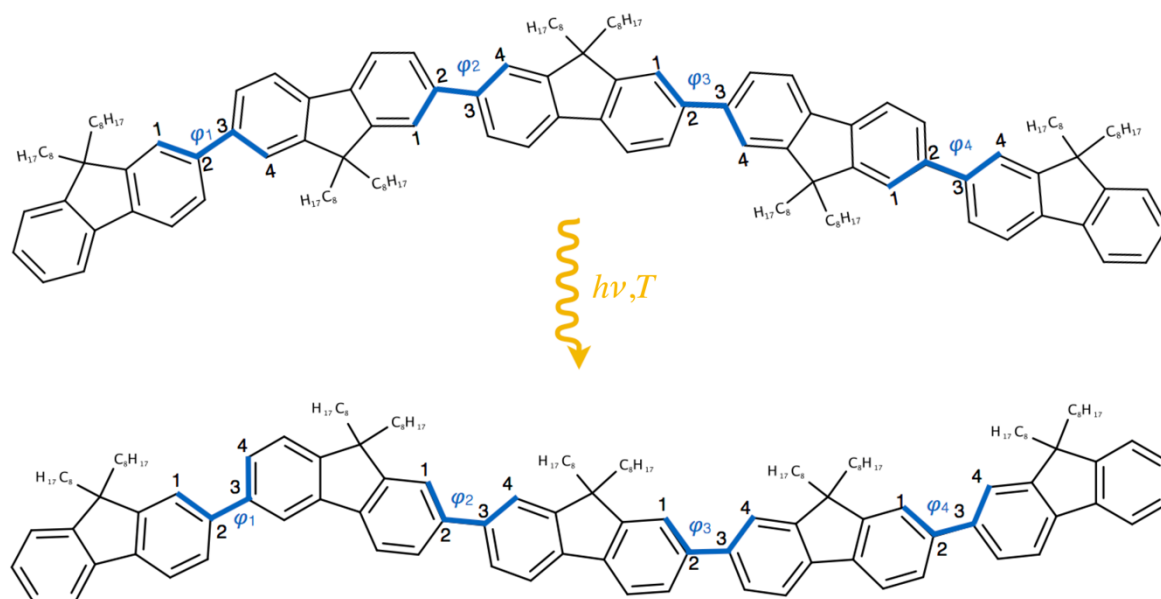
Conjugated polymers are a class of organic frameworks that are widely used in an extensive range of electronic applications, thanks to their promising optical and electronic properties.¹ These polymers offer an excellent alternative to inorganic materials since they are moderately

low-cost.² For these reasons, conjugated polymers have found remarkable applications in devices such as organic photovoltaics (OPV), organic light-emitting diodes (OLED), organic field-effect transistors (OFET) and a variety of sensors.³⁻¹² Polyfluorene derivatives are of wide interest in the field of organic electronics. A peculiarity of these systems is the photo-induced torsional reorganization around the conjugated backbone,^{13,14} through a *twisted-coplanar* transition, which allows a specific molecular response after light-irradiation.¹⁵⁻¹⁸ Several computational efforts have been performed in the last decades to predict the properties of polyfluorenes and ultimately to optimize their structural¹⁹ and optical properties,^{20,21} electronic structure²²⁻²⁴ or charge-transport character.²⁵

In 2012, *Clark et al.* have shown through non-adiabatic excited-state dynamic simulations that the photo-induced torsional relaxation around the backbone of 5-mer of 9,9-dioctylfluorene may occur in a toluene solution in a sub-100 fs timescale.²⁶ A flattening mechanism was predicted to occur during the decay, showing the conversion of the electronic potential energy into torsional kinetic energy. However, non-adiabatic excited state molecular dynamics simulations often require excited-state quantum simulations performed at every time step on an ensemble of trajectories, each propagated for a picosecond or more. Consequently, although this field has matured significantly with remarkable improvements in the simulation of very large molecular systems, it often requires to make compromises in order to find the best balance between precision and numerical cost.²⁷ Force-field based excited state simulations are promising for studying large-scale transitions occurring during photo irradiation.²⁸⁻³⁰ Various simulation frameworks have been proposed in order to derive classical force fields able to accurately describe molecules in the ground and excited states.³¹⁻³³ This is a field of active research and, for example, inclusion of more complex functional forms including the torsion dihedrals might be important for accurate studies of photo-induced processes.

Recently, we have developed a simple approach³⁴ to estimate the free-energy gap between ground and excited states of a fluorene pentamer, while at the same time enhancing the sampling of different conformers. Within this simulation framework, several sets of independent free-energy simulations are performed to enable an exhaustive sampling of the conformational space, and free-energy perturbation theory (FEP)^{35,36} is then used to provide an accurate estimate of the free-energy gap between ground and first excited state. In this work, we extend the method by biasing multiple torsions of fluorene-based oligomers substituted in the 9-position by dioctyl chains (Scheme 1), a substitution that is usually employed to improve the solubility in organic solvents. The Parallel Bias metadynamics approach³⁷ combined with Hamiltonian Replica Exchange (REM)³⁸ are used to increase the efficiency of our scheme and, in combination with FEP, characterize the free-energy

landscapes of the first singlet S_0 ground state and the lowest singlet excited states S_1 and S_2 as well as the transitions between these states.



Scheme 1. Photo-induced twisted-coplanar transition occurring on a 5-mer of 9,9-dioctylfluorene.

II. THEORETICAL FRAMEWORK

Derivation of the torsional potential

The potential energy surfaces (PES) as a function of the dihedral rotation were performed within the Density Functional Theory (DFT) framework for the torsions belonging to a fluorene pentamer in the ground and in the first two singlet excited states. The Becke's three-parameter hybrid functional (B3) with the Lee, Yang, and Parr (LYP) expression for the nonlocal correlation, B3LYP³⁹ were initially used and compared with the Coulomb-attenuating method CAM-B3LYP.⁴⁰ We compared the PES at the CAM-B3LYP/6-31G* and B3LYP/6-31G* levels of theory. We detected a shift of 0.62 eV in the S_1 state higher for the CAM-B3LYP/6-31G* and a rising of the coplanar barrier of 0.02 eV and 0.05 eV, respectively in S_0 and S_1 states, with respect to the PES calculated at the B3LYP/6-31G* level of theory. Therefore, we proceeded to compute the PES at the B3LYP/6-31G* level of theory using Gaussian16,⁴¹ in line with previous reports indicating this level of theory is suitable to predict the electronic structure of polyfluorenes.²²

The torsional conformers of the fluorene pentamer were optimized by varying each of the $\varphi_1, \varphi_2, \varphi_3$ torsions from 0 to 180 degrees in the S_0, S_1 and S_2 states. Due to the C_2 symmetric repeating unit, φ_1 is equivalent to φ_4 and φ_2 to φ_3 . While in the ground state the E^{QM} values

of the PES of the consecutive torsions does not show appreciable differences, in the excited states the external (φ_1) and the internal torsion (φ_2) or (φ_3) markedly vary (Figure 1 and Figure S6-S8). In particular, the PES of the second torsion (φ_2) shows lower energy values for coplanar conformers and a higher potential energy barrier at 90 degrees that increases owing to the loss of conjugation, with respect to the PES of the first torsion (φ_1). Coplanar states are stabilized through light irradiation owing to the lowering of the potential energy barriers at 0 degrees in S_1 and S_2 excited states and to the increase of the potential energy barrier at 90 degrees. Consequently, we derived two sets of torsional potentials for the external and the internal torsions of the polymer. Non-linear least-square interpolations were performed by minimizing the square difference ΔE between the molecular mechanics energies (E^{MM}) and the *ab initio* energies (E^{QM}) for the N points on the PES of the electronic state i , reported in Eq. 1.

$$\Delta E_i = \sum_{j=1}^N (E^{QM_i}(\varphi_j) - E^{MM_i}(\varphi_j))^2 \quad (1)$$

where:

$$E^{MM_i}(\varphi) = E^{CHARMM} + V^{S_i}(\varphi) + \sum K_m(1 + \cos(m\phi - \phi_0)) \quad (2)$$

and:

$$V^{S_i}(\varphi) = \sum_{n=0}^5 C_n^{S_i} (\cos(\varphi - 180))^n \quad (3)$$

in which E^{CHARMM} represents the force-field potential CHARMM CGenFF⁴² and $V^{S_i}(\varphi)$ represents the torsional potential in a given electronic state i related to the torsions for which each PES is calculated (φ is defined as 1234 from Scheme 1).

The term K_m and ϕ_0 represent the force constants and the phase of a cosine series describing the other proper ϕ dihedral acting on the fluorene-fluorene rotation. The values of E^{MM} were calculated from an energy minimization of the optimized coordinates of the QM PES. We also tested the fitting parameters through the torsional free-energy profiles calculated at 200 K, where the free energy approaches the PES (Figure 1). The K_m and ϕ_0 terms of the proper dihedrals were calculated with iterative fits starting from $K_m = 0$ and using as initial guess the fitting parameters from the QM PES interpolation for the φ torsion in a given electronic state. As shown in the free-energy profiles reconstructed at 200 K, together with the potential energy minimization (the oscillations in the angles mostly derived from the minimization algorithm), the K_m and ϕ_0 terms found for the ground-state combined with the fitting parameters of the QM PES in a given electronic state, well reproduced the potential energy along the φ torsion (Figure 1).

The fitting parameters describing the $V^{S_i}(\varphi)$ potential are reported in Table 1, the parameters describing the proper dihedrals are reported in Table 2. The ESP charges were calculated for

each optimized electronic state of the 5-mer oligofluorene at the B3LYP/6-31G* and are reported in Tables S1 of Supplementary Material. We also calculated the ESP charges at the MP2⁴³ and CIS⁴⁴ level of theory. Those are consistent with the ones derived at the B3LYP/6-31G* level of theory and are reported in Table S2 of the Supplementary Material.

Table 1. The coefficients $C_n^{S_i}$ (kJ/mol) of the Ryckaert-Bellemans function described in Eq. 3 and used in GROMACS, obtained through a non-linear least-square interpolation of the PES values obtained at the B3LYP/6-31G* level.

C_0	C_1	C_2	C_3	C_4	C_5
$S_0(\phi)$					
12.16	-0.02400	-43.32	0.1200	38.80	-0.06010
$S_1(\phi_1)$					
301.3	-0.1478	-48.16	0.9948	34.30	-1.001
$S_2(\phi_1)$					
348.8	-0.1104	-54.71	0.7533	35.14	-0.8068
$S_1(\phi_2)$					
313.9	0.3972	-72.12	-0.9463	43.87	0.5858
$S_2(\phi_2)$					
351.9	-0.7135	-69.01	0.653	47.11	0.41

Table 2. Torsional parameters for the proper dihedrals ϕ described in Eq. 2, including one multiple cosine function and two single cosine functions.

K_m (kJ/mol)	ϕ_0	m
-6.40	180	4
2.20	180	2
-8.20	0.0	4
-2.20	0	2
-2.20	0	2

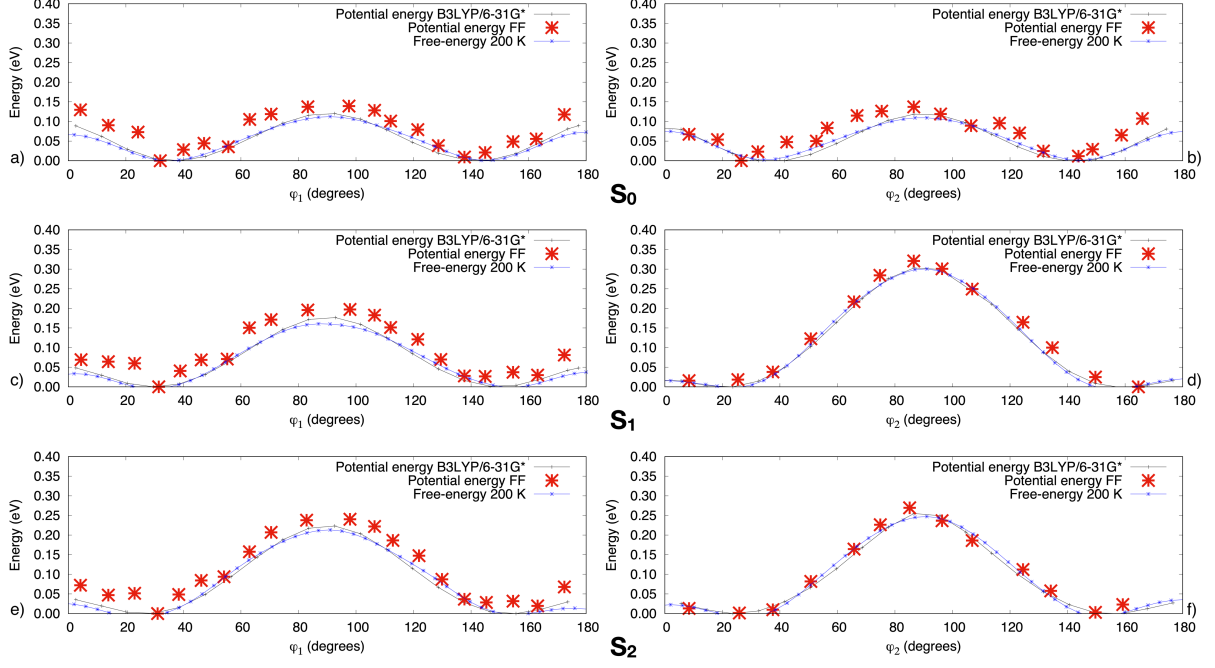


Figure 1. Fluorene-fluorene torsional potential calculated from energy-minimized conformations at MM level and from free energy calculated with Well-tempered metadynamics simulations at 200 K. The total energy calculated at B3LYP/6-31G* level of theory is also shown. a) Calculations related to the torsion (φ_1) of the fluorene pentamer in the S_0 state, b) calculations related to the torsion (φ_2) of the fluorene pentamer in the S_0 state, c) calculations related to the torsion (φ_1) of the fluorene pentamer in the S_1 state, d) calculations related to the torsion (φ_2) of the fluorene pentamer in the S_1 state, e) calculations related to the torsion (φ_1) of the fluorene pentamer in the S_2 state, f) calculations related to the torsion (φ_2) of the fluorene pentamer in the S_2 state.

Hamiltonian Replica Exchange combined with Free-energy perturbation

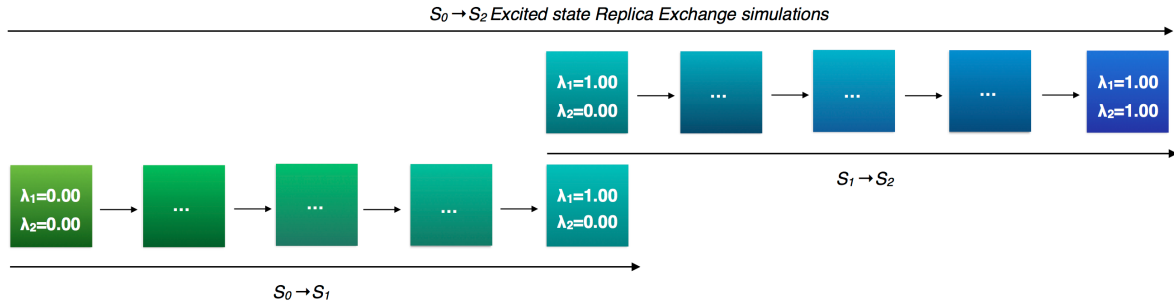
The free-energy as a function of the fluorene-fluorene dihedral angles φ_i is defined as follows:

$$F^{S_i}(\varphi_i) = -\frac{1}{\beta} \log \left(\frac{\int \delta(\varphi_i - \varphi_i(\mathbf{r})) e^{-\beta V(\mathbf{r})} d\mathbf{r}}{\int e^{-\beta V(\mathbf{r})} d\mathbf{r}} \right) \quad (4)$$

In this equation, $V(\mathbf{r})$ represents the interatomic potential (the force field), \mathbf{r} the atomic coordinates, and β represents the inverse of $k_B T$, where k_B is the Boltzmann constant and T the temperature of the system. We now add to the interatomic potential the torsional potential reported $V^{S_i}(\varphi_i)$ defined in Eq.3. Hence, the free-energy surface for a given electronic state $F^{S_i}(\varphi_i)$ becomes:

$$F^{S_i}(\varphi_i) = -\frac{1}{\beta} \log \left(\frac{\int \delta(\varphi_i - \varphi_i(\mathbf{r})) e^{-\beta (V(\mathbf{r}) + V^{S_i}(\varphi_i(\mathbf{r})))} d\mathbf{r}}{\int e^{-\beta (V(\mathbf{r}) + V^{S_i}(\varphi_i(\mathbf{r})))} d\mathbf{r}} \right) \quad (5)$$

In order to evaluate the free-energy difference between the S_0 , S_1 and S_2 electronic states, FEP was used in combination with REM, following the approach introduced in Ref.⁴⁵. Multiple intermediate windows between the S_0 , S_1 and S_2 electronic states were introduced through two parameters λ_1 and λ_2 . The former is used to reach S_1 from S_0 ($\lambda_1: 0 \rightarrow 1$; $\lambda_2 = 0$); the latter to reach S_2 from S_1 ($\lambda_1 = 1$; $\lambda_2: 0 \rightarrow 1$) (Scheme 2).



Scheme 2. Scheme of the simulation framework herein proposed based on Hamiltonian Replica Exchange, where each replica differs from the torsional potentials through λ_1 and λ_2 parameters. Each torsion is biased within the parallel bias metadynamics approach.

The external potential acting on each replica is defined as:

$$V_\lambda(\varphi) = \sum_{m=1}^4 [(1 - \lambda_1)V^{S_0}(\varphi_m) + \lambda_1(1 - \lambda_2)V^{S_1}(\varphi_m) + \lambda_2V^{S_2}(\varphi_m)] \quad (6)$$

Where m represents the number of torsions belonging to the polymer. In order to obtain an adequate overlap between the energy distributions of adjacent windows, a step sizes $\Delta\lambda_1$ equal to 0.04 and $\Delta\lambda_2$ equal to 0.1 were used for the S_0 - S_1 and S_1 - S_2 transitions, respectively. The step size was chosen as a compromise between achieving an overlap between torsional potentials of neighboring replicas and keeping the simulation cost moderate (i.e. the minimum number of λ windows to allow an overlap between torsional potentials).

In this REM framework, N non-interacting replicas of the system, each identified by a given pair $\lambda = (\lambda_1, \lambda_2)$ of control parameters, were simulated in parallel. At fixed time intervals, a swap between two configurations belonging to neighboring replicas was attempted and accepted using a Metropolis criterion based on the overlap between energy distributions of the two replicas. The use of the different (λ_1, λ_2) intermediate windows makes possible an efficient exchange between replicas. In this way, instead of multiple independent FEP runs, the simulation can be executed in a single multi-replica run. Within this framework, the ground state replica with higher coplanar free-energy barriers can be exchanged with excited state replica having lower coplanar free-energy barriers, thus enhancing sampling. Furthermore, the overlap between energy distributions of neighboring replicas, which is ensured to obtain efficient diffusion in the $\lambda = (\lambda_1, \lambda_2)$ space, guarantees also an accurate calculation of the free-energy difference between two neighboring replicas using the FEP approach in Eq. 7:

$$\Delta F^{(\lambda_i+\Delta\lambda)} = -\frac{1}{\beta} \log \langle e^{-\beta(V_{\lambda_i+\Delta\lambda}-V_{\lambda_i})} \rangle_{\lambda_i} \quad (7)$$

Finally, the free-energy gap between the S_0 and S_1 and S_1 and S_2 electronic states can be estimated as the sum over the free-energy differences between neighboring replicas using Eq. 8:

$$\Delta F^{S_i \rightarrow S_{i+1}} = \sum_i \Delta F^{(\lambda_i+\Delta\lambda)} \quad (8)$$

where the free-energy gap has been divided by the number of torsions.

Enhanced sampling with Parallel Bias metadynamics.

Parallel Bias metadynamics (PBMetaD)³⁷ was used to enhance sampling in each REM replica. The four main-chain dihedrals belonging to the polymer ($\varphi_1, \varphi_2, \varphi_3, \varphi_4$) were used as Collective Variables (CVs). Multiple mono-dimensional metadynamics⁴⁶ bias potentials $V_G(\varphi_i; t)$ were used to construct the PBMetaD bias potential $V_{PB}(\varphi_1, \varphi_2, \varphi_3, \varphi_4; t)$ defined by:

$$V_{PB}(\varphi_1, \varphi_2, \varphi_3, \varphi_4; t) = -\frac{1}{\beta} \log \left(\sum_{i=1}^4 e^{-\beta V_G(\varphi_i; t)} \right) \quad (9)$$

The individual metadynamics potential $V_G(\varphi_i; t)$ is built adaptively during the course of the simulation by depositing Gaussian functions along the system trajectory in the CVs space:

$$V_G(\varphi_i; t) = \int_0^t dt' \omega(t') \cdot \exp \left(-\frac{(\varphi_i(r) - \varphi_i(r(t')))^2}{2\sigma_i^2} \right) \quad (10)$$

where t is simulation time, σ_i the Gaussian width of the i -th CV, and ω the deposition rate of the bias potential. Typically, Gaussians are added to the simulation with a discrete and constant deposition stride τ . Therefore, the deposition rate ω is expressed as the ratio between the Gaussian height W and the deposition stride τ . Similarly to well-tempered metadynamics,⁴⁷ in PBMetaD the Gaussian height decreases with simulation time as:

$$W(t) = W_0 \cdot \exp \left(-\frac{V_G(\varphi_i; t)}{k_B \Delta T} \right) \cdot \frac{e^{-\beta V_G(\varphi_i; t)}}{\sum_{i=1}^4 e^{-\beta V_G(\varphi_i; t)}} \quad (11)$$

where W_0 is the initial Gaussian height and ΔT an input parameter with the dimension of a temperature.

ΔT can be used to limit the exploration to relevant regions of the CV space and thus avoid visiting excessively high free-energy areas. This parameter is often expressed in terms of the so-called biasfactor:

$$\gamma = \frac{T+\Delta T}{T} \quad (12)$$

At convergence, one-dimensional free-energy profiles $F(\varphi_i)$ can be reconstructed directly from the bias potentials $V_G(\varphi_i; t)$ as in standard well-tempered metadynamics simulations:

$$V_G(\varphi_i; t \rightarrow \infty) = -\frac{\Delta T}{T+\Delta T} \cdot F(\varphi_i) + C \quad (13)$$

while multi-dimensional free-energy surfaces can be reconstructed by reweighting.⁴⁸ The presence of the PBMetaD bias potential $V_{PB}(\varphi_1, \varphi_2, \varphi_3, \varphi_4; t)$ was accounted for when calculating the swap acceptance probability in the REM scheme as well as when computing the FEP ensemble average in Eq. 7.

Simulation Details

The initial 5-mer of 9,9-dioctylfluorene structures were built by selecting the polymeric chains from the simulated system reported in Ref.⁴⁹

In order to derive the force field in the ground and excited states, potential energy scans as a function of the dihedral rotation of the unsubstituted fluorene pentamer were carried out using the Density Functional Theory (DFT) framework with the B3LYP³⁹ functionals and the 6-31G* basis set within the Gaussian16 package.⁴¹ The torsional conformers were optimized varying the torsion from 0 to 180 degrees in the S_0 and S_1 states.

Subsequently, the initial coordinates were energy-minimized *in vacuo* using the Steepest Descent Algorithm and equilibrated *in vacuo* at 200 K and at 300 K using the *ab initio* derived torsional potential combined with the CHARMM based General Force Field.⁴² The equilibrated conformation at 200 K was used as starting coordinates for reconstructing the free-energy profile at 200 K. Specifically, two well-tempered metadynamics⁴⁷ runs were carried out using the first (external) or the second (inner) polyfluorene dihedrals. Gaussians with initial height equal to 1.2 kJ/mol and with width of 0.2 radians, were deposited with a stride of 1 ps and biasfactor equal to 25 in order to allow an efficient diffusion among replicas, with a temperature of 300 K.

The equilibrated conformation at 300 K was used as starting coordinates for the REM simulations. 36 replicas were used: 26 to cover the interval S_0 , S_1 and 10 for the interval S_1 ,

S_2 . Each replica was simulated in the NVT ensemble at 300 K enforced by the velocity rescaling thermostat.⁵⁰

A swap between two neighboring replicas was attempted every 100 MD steps and accepted using a Metropolis criterion. For the PBMetaD approach, Gaussians with initial height equal to 1.2 kJ/mol were deposited with a stride of 1 ps and biasfactor equal to 40. The simulation length of each replica was 0.085 μ s, for a total aggregated simulation time of 3.06 μ s.

In all simulations, the time step was set at 2 fs. The LINCS algorithm⁵¹ was used to fix all bonds lengths. For the Lennard-Jones and electrostatic interactions, a cutoff of 2.0 nm was used. The Particle Mesh Ewald method⁵² was used to calculate electrostatic interactions. Periodic boundary conditions were applied using a cell dimension of 48.140x64.085x16.445 nm³ with a system size of 347 atoms. All simulations were performed with GROMACS 2020.2⁵³ equipped with PLUMED 2.7.0.⁵⁴ The conformations sampled in the S_1 state have been clustered with torsional angles ranging from 20 to 155 degrees. The oscillator strengths have been computed for those selected coordinates using the ZIndo/S method^{55,56} as implemented in Gaussian 16 package,⁴¹ and subsequently scaled with the square of each wavenumbers. The calculations of the emission spectra at a given emission energy were carried out assuming Gaussian bands with 50 cm⁻¹ full width at half-height for all transitions centered in a given emission energy converted in wavenumbers.

III. FREE-ENERGY PATHWAYS IN THE GROUND AND EXCITED STATES

The free-energy profiles reconstructed for a 5-mer of 9,9-dioctylfluorene as a function of the dihedral angles ($\varphi_1, \varphi_2, \varphi_3, \varphi_4$) and concerning the S_0, S_1 and S_2 states are shown in Figure 2. Inspection of the simulated free-energy profiles at 300 K pointed out striking differences with the adiabatic PES computed at the *ab-initio* level (shown in Figure 1). First, the minima at 44 degrees and 155 degrees, which were predicted to be degenerate in the former PES (Figure 1), showed in the free-energy profiles different stabilities of 0.14 eV in the S_0 state and 0.15 eV in S_1 and S_2 states (Figure 2). Second, the coplanar barrier decreased by 0.05 eV in S_1 and 0.06 eV in S_2 free-energy profiles with respect to those of the ground state (Figure 2). No significant differences have been observed in the free-energy profiles of the ground state as a function of the $\varphi_1, \varphi_2, \varphi_3, \varphi_4$ dihedrals.

Small variations appear in the free-energy profiles of the excited states. The S_1 state shows different orthogonal free-energy barrier at 90 degrees on the external and internal torsions (0.22 eV for φ_1 , 0.34 eV for φ_2 , 0.33 eV for φ_3 and 0.24 for φ_4), whereas the S_2 state shows variations in the coplanar free-energy barrier (0.03 eV for φ_1 or φ_4 ; 0.09 eV for φ_2 and 0.11 eV for φ_3).

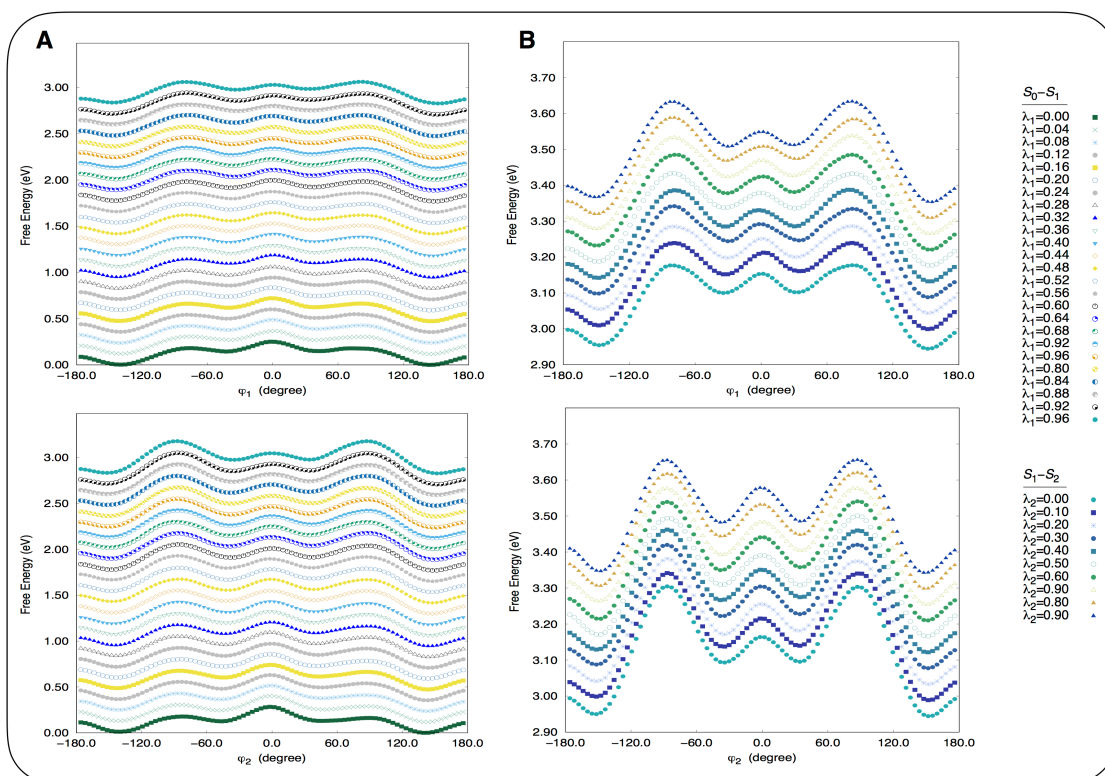


Figure 2. **A.** Free-energy profiles computed using the Parallel Bias metadynamics approach combined with Hamiltonian Replica Exchange, as a function of the dihedral angles φ_1 , φ_2 and for the S_1-S_0 transition. **B.** Free-energy profiles for the S_2-S_1 transition as a function of the dihedral angles φ_1 , φ_2 .

The calculated S_1-S_0 free-energy gap estimated by FEP is equal to 2.946 eV, while the calculated S_1-S_2 free energy gap is predicted as 0.442 eV, both with a statistical error of 2×10^{-4} eV. Notably, the calculated S_1-S_0 free-energy gap shows a good agreement with the experimental photoluminescence spectrum centered at 2.88 eV reported for a 5-mer of 9,9-dioctylfluorene.⁵⁷ Since we derived relaxed QM PES, we predicted emission free-energy estimates and those turn out to be slightly higher than the experimental one ($2.946 \pm 2 \times 10^{-4}$ eV vs 2.88 eV). Indeed, this protocol can be straightforwardly extended to absorption processes, by fitting a Franck-Condon vertical transition from the ground state instead of a relaxed PES, as in this case.

At variance with an unsubstituted 5-mer oligofluorene in which the free-energy landscape is characterized by four degenerate free-energy minima,³⁴ the dioctyl chains stabilize the dihedral values of 155 degrees close to the values of 144 degrees typical of a 5_2 helix, instead of the values of 72 degrees typical of a 5_1 helix. The more favorable packing for a 5_2 helix instead of a 5_1 helix was previously suggested from electron diffraction patterns combined with geometry optimizations at RHF/6-31G(d,p) level of theory.⁵⁸ The 5_2 helix is further stabilized

in the S_1 and S_2 excited states where a higher orthogonal free-energy barrier at 90 degrees is observed for the free-energy profiles reconstructed along the first φ_1 dihedral of S_1 and S_2 states (0.23 eV and 0.28 eV, respectively) compared to the free-energy barrier of 0.18 eV in the one of S_0 .

A *switch* region is detected at values of angles of 44 degrees, where a reduced free-energy coplanar barrier is observed for the φ_1 transition towards a coplanar state (~ 0.04 eV) with respect to that belonging to the ground state (~ 0.10 eV). Notably, the dihedral angles of the absolute free-energy basins in S_1 and S_2 states are shifted towards higher values approaching 155 degrees, whereas the dihedral angles of the *switch* free-energy basin are stabilized towards values approaching 27 degrees (Figure 2), favoring in this way a molecular switch from positive to coplanar dihedrals reaching negative twist dihedrals (Figure 3). These results are in agreement with the typical twisted-coplanar transition of biphenyl-based rotors, herein represented in the molecular conformations sketched in Figure 3 for S_0 , S_1 and S_2 electronic states. In particular, the free-energy surfaces reconstructed for S_0 , S_1 and S_2 states as a function of two consecutive dihedrals are highlighted in Figure 3, together with the relative switching pathway. From those isosurfaces, the minimal free-energy pathway is predicted to occur through the torsion periodicity at 180 degrees, allowing the dihedral inversion of the most stable conformer with 155 degrees (path from A to C). The barriers at 180 degrees progressively decrease going from the S_0 to S_1 and S_2 states, as highlighted in the monodimensional free-energy profiles reconstructed aligning the horizontal (C-B transition) and vertical (A-B transition) paths along φ_1 and φ_2 or φ_2 and φ_3 (Figure 3). Noteworthy, S_1 and even more S_2 were predicted to stabilize coplanar dihedrals, with a local free-energy minimum located at ± 44 degrees far from the global free-energy minimum at 155 degrees.

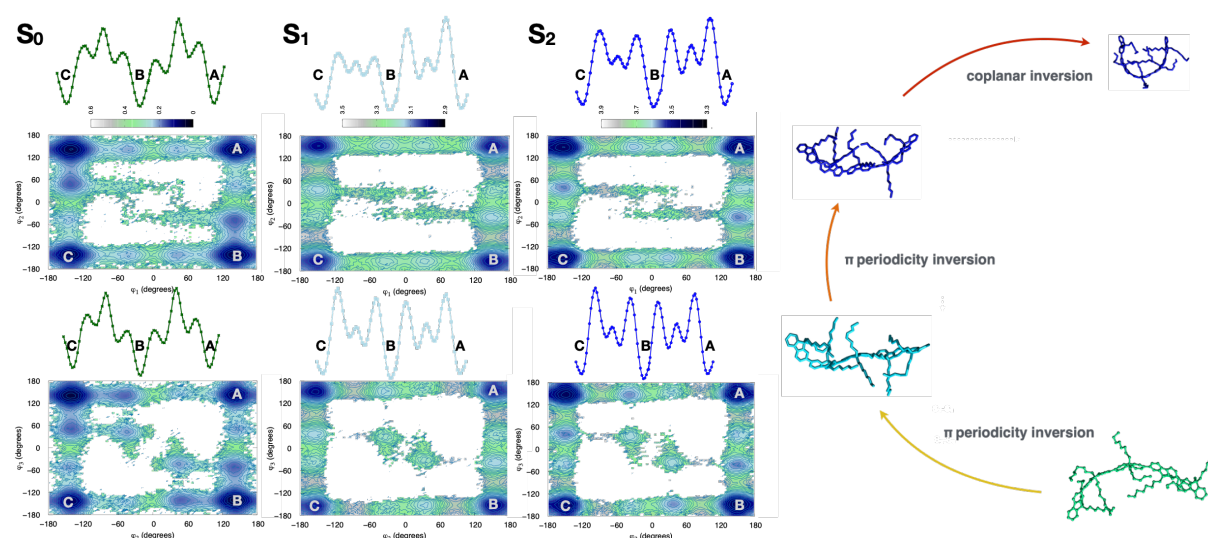


Figure 3. Free-energy isosurfaces reconstructed as a function of the φ_1 and φ_2 dihedrals, with the monodimensional free-energy profiles representing C-B and A-B transition. The photoswitchable mechanism from S_0 to S_2 is shown and predicted with a π -periodicity inversion.

We finally assessed the proposed mechanism through the calculation of the emission spectrum (Figure 4). The predicted emission spectrum, despite being shifted by 0.06 eV with respect to the experimental profile reported by Kang et al.,⁵⁷ presents a similar shape with two main central peaks. Our multidimensional free-energy surfaces suggest a photoswitchable transition starting from the free-energy minimum approaching the 5_2 helix conformation. Upon irradiation the 5-mer of 9,9-dioctylfluorene can invert its dihedrals through the π -periodicity. A further transition can undergo away from the global free-energy minimum in the S_1 and in S_2 state, where the coplanar dihedrals and the conformers located at ± 44 degrees are stabilized by higher free-energy barriers (0.03 eV for S_0 , 0.08 eV for S_1 , 0.12 eV for S_2). Noteworthy, from a direct comparison with the free-energy simulations of the 5-mer of unsubstituted fluorene and the 5-mer of 9,9-dioctylfluorene, the helix inversion is predicted to be more favored in alkyl substituted oligofluorenes where the dihedral values towards 155 degrees are more stable with respect to the unsubstituted ones.

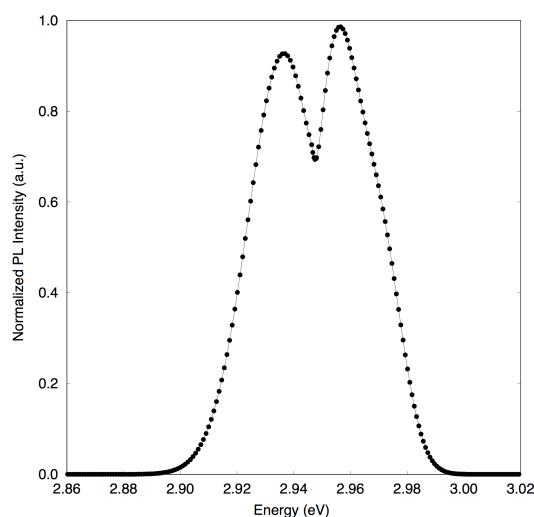


Figure 4. Calculated emission spectra from the S_1 - S_0 emission free-energies calculated within the REM/PBMetaD/FEP scheme. The intensity has been predicted via the calculation of the transition dipole moments at the ZINDO/S level, from the coordinates belonging to the S_1 state sampled within the REM/PBMetaD/FEP scheme.

IV. CONCLUSIONS

In summary, we have introduced a simulation scheme that combines Hamiltonian Replica Exchange, Parallel Bias metadynamics and the free-energy perturbation theory to enhance sampling of the conformational space of a switchable 5-mer of 9,9-dioctylfluorene and at the same time to estimate the free-energy gaps between ground and excited states. The simulation framework presented here is particularly indicated when thermal effects

accompany the irradiation process. Two different photoswitchable pathways were discussed. Specifically, with an excitation to the first excited state, a dihedral switching from the absolute free-energy minimum identifying a conformation with dihedrals at 155 degrees was predicted. From the S_1 state, a further transition can drive the 5-mer of 9,9-dioctylfluorene away from the global free-energy minimum, reaching the S_2 state and allowing the oligomer to decay in ± 44 degrees twisted conformations.

Furthermore, the method predicted with good accuracy the emission spectrum and pointed out the highest stability in the ground state of a 5_2 helix conformation compared to a 5_1 helix one.

This biasing scheme presented here is general and can be used to predict large-scale rearrangements occurring through light-matter interactions, particularly when thermal effects are relevant for the occurrence of photoswitchable twisted-coplanar transitions in excited states.

SUPPLEMENTARY MATERIAL

See the supplementary material for the evolution of all dihedral angles during the time (Figure S1-S3), replica diffusions during the simulations (Figure S4), the free-energy profiles as a function of φ_3, φ_4 (Figure S5), the benchmarked potential energy scans (Figure S6-S8), the values of potential energy scans (Tables S1,S2) and ESP charges (Tables S3 and S4).

DATA AVAILABILITY STATEMENT

All the GROMACS input and topology files as well as the PLUMED input files used in this study are available on PLUMED-NEST (www.plumed-nest.org), under accession id plumID:21.008.

ACKNOWLEDGMENTS

The ISCRA supercomputing initiative is acknowledged for computational time provided. This research was funded by Italian Ministry of Research under the program PRIN2017 no. 2017WBZFHL_003 (AP).

References

1. Y. Tsuji, Y. Morisaki, Y. Chujo, *Polymer Journal* **49**, 203 (2017).
2. R.M. Pankow, B. C. Thompson, *Polymer* **207**, 122874 (2020).

3. R. Noriega, J. Rivnav, K. Vandewall, F.P.V. Koch, N. Stingelin, P. Smith, M.F. Toney, A. Salleo, *Nat Mater.* **12** (11), 1038 (2013).
4. A. Facchetti, *Chem. Mater.* **23** (3), 733 (2011).
5. A. Grimsdale, K.L. Chan, R.E. Martin, P.G. Jokisz, A. B. Holmes, *Chem. Rev.* **109** (3), 897 (2009).
6. J. Clark, G. Lanzani, *Nature Photon.* **4**, 438 (2010).
7. B. K. Yap, R. D. Xia, M. Campoy-Quiles, P. N. Stavrinou, D. D. C. Bradley, *Nature Mater.* **7**, 376 (2008).
8. T. Virgili, D. Marinotto, C. Manzoni, G. Cerullo, G. Lanzani, *Phys. Rev. Lett.* **94**, 117402 (2005).
9. K. C. Vishnubhatla, J. Clark, G. Lanzani, R. Ramponi, R. Osellame, T. Virgili, *Appl. Phys. Lett.* **94**, 041123 (2009).
10. D. Kabra, L. P. Lu, M. H. Song, H. J. Snaith, R. H. Friend, *Adv. Mater.* **22**, 3194 (2010).
11. G. Albano, G. Pescitelli, L. Di Bari, *Chem. Rev.* **120**, 18, 10145 (2020).
12. C. R. McNeill, N. C. Greenham, *Adv. Mater.* **21**, 3840 (2009).
13. Y. Wang, T. Sakamoto, T. Nakano, *Chem. Commun.*, **48**, 1871(2012).
14. Y. Wang, T. Harada, L. Q. Phuong, Y. Kanemitsu, T. Nakano, *Macromolecules* **51** (17), 6865 (2018).
15. A. Pietropaolo, T. Nakano, *J. Am. Chem. Soc.* **135**, 5509 (2013).
16. A. Pietropaolo, S. Tang, F. M. Raymo, *Nanoscale*, **9** 4989 (2017).
17. L. Angiolini, L. Giorgini, H. Li, A. Golemme, F. Mauriello, R. Termine, *Polymer* **51**, 368 (2010).
18. L. Angiolini, T. Benelli, L. Giorgini, F. Mauriello, E. Salatelli, R. Bozio, A. Daurù, D. Pedron, *Eur. Polym. J.* **43**, 3550 (2007).
19. V. Marcon, N. van der Vegt, G. Wegner, G. Raos, *J. Phys. Chem. B* **110**, 5253 (2006).
20. W. Chunwaschirasiri, B. Tanto, D. L. Huber, M. J. Winokur, *Phys. Rev. Lett.* **94**, 107402 (2005).
21. X. K. Chen, Y. Tsuchiya, Y. Ishikawa, C. Zhong, C. Adachi, J. L. Bredàs, *Adv. Mater.* **29**, 1702767 (2017).
22. S. Kilina, E. R. Batista, P. Yang, S. Tretiak, A. Saxena, R. L. Martin, D. L. Smith, *ACS Nano* **2**, 1381 (2008).
23. T. Körzdörfer, J. L. Bredàs, *Acc. Chem. Res.* **47**, 3284 (2014).
24. E. Fron, A. Deres, S. Rocha, G. Zhou, K. Müllen, F. C. De Schryver, M. Sliwa, H. Uji-i, J. Hofkens, T. Vosch, *J. Phys. Chem. B* **114**, 1277 (2010).
25. J. S. Kim, L. Lu, P. Sreearunothai, A. Seeley, K. H. Yim, A. Petrozza, C. E. Murphy, D. Beljonne, J. Cornil, R. H. Friend, *J. Am. Chem. Soc.* **130**, 13120 (2008).

26. J. Clark, T. Nelson, S. Tretiak, G. Cirimi, G. Lanzani, *Nat. Phys.*, **8**, 225 (2012).
27. T. R. Nelson, A. J. White, J. A. Bjorgaard, A. E. Sifain, Y. Zhang, B. Nebgen, S. Fernandez-Alberti, D. Mozyrsky, A.E. Roitberg, S. Tretiak, *Chem. Rev.* **120**, 2215 (2020).
28. J. Sjöqvist, M. Linares, K.V. Mikkelsen, P. Norman, *J Phys Chem A.*, **118(19)**, 3419 (2014).
29. J. Sjöqvist, R.C. González-Cano, J.T. López Navarrete, J. Casado, M.C. Ruiz Delgado, M. Linares, P. Norman, *Phys Chem Chem Phys.*, **16(45)**, 24841 (2014).
30. T. Northey, J. Stacey, T. J. Penfold, *J. Mater. Chem. C*, **5**, 11001 (2017).
31. O. Andreussi, I. G. Prandi, M. Campetella, G. Prampolini, B. Mennucci, B., *J. Chem.Theory Comput.*, **13**, 4636 (2017).
32. G. Prampolini, P. R. Livotto, I. Cacelli, *J. Chem. Theory Comput.*, **11**, 5182 (2015).
33. I. Cacelli, G. Cinacchi, G. Prampolini, A. Tani, *J. Am. Chem. Soc.*, **126**, 14278 (2004).
34. C. Cozza, M. Bonomi, A. Pietropaolo, *J. Chem. Theory Comput.*, **14**, 5441 (2018).
35. W.L Jorgensen, L.L. Thomas, *J Chem Theory Comput.* **4**, 869 (2008).
36. B. W. J. Irwin, *J. Chem. Theory Comput.* **14**, 3218 (2018).
37. J. Pfaendtner, M. Bonomi, *J. Chem. Theory Comput.* **11**, 5062 (2015).
38. Y. Sugita, Y. Okamoto, *Chem. Phys. Lett.* **314**, 141–151 (1999).
39. P.J. Stephens, F.J.Devlin. C.F. Chabalowski, M.J. Frisch, *J.Phys.Chem.* **98**, 11623 (1994).
40. T. Yanai, D. Tew, N. Handy, *Chem. Phys. Lett.*, **393**, 51, (2004)
41. Gaussian 16, Revision C.01, M. J. Frisch, G. W. Trucks, H. B. Schlegel, G. E. Scuseria, M. A. Robb, J. R. Cheeseman, G. Scalmani, V. Barone, G. A. Petersson, H. Nakatsuji, X. Li, M. Caricato, A. V. Marenich, J. Bloino, B. G. Janesko, R. Gomperts, B. Mennucci, H. P. Hratchian, J. V. Ortiz, A. F. Izmaylov, J. L. Sonnenberg, D. Williams-Young, F. Ding, F. Lipparini, F. Egidi, J. Goings, B. Peng, A. Petrone, T. Henderson, D. Ranasinghe, V. G. Zakrzewski, J. Gao, N. Rega, G. Zheng, W. Liang, M. Hada, M. Ehara, K. Toyota, R. Fukuda, J. Hasegawa, M. Ishida, T. Nakajima, Y. Honda, O. Kitao, H. Nakai, T. Vreven, K. Throssell, J. A. Montgomery, Jr., J. E. Peralta, F. Ogliaro, M. J. Bearpark, J. J. Heyd, E. N. Brothers, K. N. Kudin, V. N. Staroverov, T. A. Keith, R. Kobayashi, J. Normand, K. Raghavachari, A. P. Rendell, J. C. Burant, S. S. Iyengar, J. Tomasi, M. Cossi, J. M. Millam, M. Klene, C. Adamo, R. Cammi, J. W. Ochterski, R. L. Martin, K. Morokuma, O. Farkas, J. B. Foresman, and D. J. Fox, Gaussian, Inc., Wallingford CT, 2016
42. K. Vanommeslaeghe, E. Hatcher, C. Acharya, S. Kundu, S. Zhong, J. Shim, E. Darian, O. Guvench, P. Lopes, I. Vorobyov, A. D. Jr.MacKerell, *J. Comput. Chem.* **31**, 671 (2010).

43. M. J. Frisch, M. Head-Gordon, J. A. Pople, Chem. Phys. Lett., **166** 275-80 (1990).
44. J. B. Foresman, M. Head-Gordon, J. A. Pople, M. J. Frisch, J. Phys. Chem., **96**, 135-49 (1992).
45. Schrödinger Release 2020-4: FEP+, Schrödinger, LLC, New York, NY, 2020.
46. A. Laio, M. Parrinello, Proc Natl Acad Sci U S A, **99**, 12562 (2002).
47. A. Barducci, G. Bussi, M. Parrinello, Phys Rev Lett., **100**, 020603 (2008).
48. G. M. Torrie, J. P. Valleau, J. Comput. Phys. **23**, 187 (1977).
49. A. Pietropaolo, Y. Wang, T. Nakano, Angew. Chem. Int. Ed. **54**, 2688 (2015).
50. G. Bussi, D. Donadio, M. Parrinello, J. Chem. Phys. **126**, 014101 (2007).
51. B. Hess, J. Chem. Theory Comput. **4**, 116 (2008).
52. U. Essmann, L. Perera, M.L. Berkowitz, T. Darden, H. Lee, L.G. Pedersen, J. Chem Phys. **103**, 8577 (1995).
53. B. Hess, C. Kutzner, D. van der Spoel, E. Lindahl, J. Chem. Theory Comp. **4**, 435 (2008).
54. The PLUMED consortium, Nat. Methods, **16**, 670 (2019).
55. J. E. Ridley, M. C. Zerner, Theor. Chim. Acta, **32**, 111 (1973).
56. J.E. Ridley, M.C. Zerner, J. Mol. Spectrosc., **50**, 457 (1974).
57. J. Kang, J. Jo, Y. Jo, S. Y. Lee, P. E. Keivanidis, G. Wegner, D. Y. Yoon, Polymer, **49**, 5700 (2008).
58. G. Lieser, M. Oda, T. Miteva, A. Meisel, H.G. Nothofer, U. Scherf, D. Neher, Macromolecules, **33**, 4490(2000).